

Violation of the orbital depairing limit in a non-unitary state —on the high field phase in the heavy Fermion superconductor UTe_2 —

Kazushige Machida

Department of Physics, Ritsumeikan University, Kusatsu 525-8577, Japan

(Dated: January 24, 2023)

A theoretical study is reported on the origin of extremely high upper critical field $\sim 70\text{T}$ observed in UTe_2 with the transition temperature $T_c=1.6\text{K}-2\text{K}$, far exceeding the conventional orbital depairing limit set by the Fermi velocity and T_c for a superconductor (SC) in the clean limit. We investigate possible violation of the orbital limit in terms of a spin-triplet nonunitary state, which is effectively coupled to the underlying magnetization induced by external field. This in turn produces the reduced internal field by cancelling it via magnetization. We formulate a theory within Ginzburg-Landau framework to describe this orbital limit violation and analyze experimental data on the upper critical fields for various field orientations in UTe_2 . It is pointed out that the orbital limit violation for a spin-triplet SC together with the Pauli-Clogston limit violation for a spin-singlet SC constitutes a complete and useful framework to examine the high field physics in superconductors in the clean limit.

PACS numbers: 74.70.Tx, 74.20.-z, 74.25.-q

I. INTRODUCTION

Much attention has been focused on a recently found heavy Fermion superconductor UTe_2 because of a candidate material of a triplet pairing, which is quite rare except for superfluid $^3\text{He}^{1,2}$ and UPt_3^{3-6} . They are all characterized by multiple phases due to rich internal degrees of freedom inherent to a spin-triplet pairing. UTe_2 is known to exhibit remarkable superconducting (SC) properties in addition to multiple phases in magnetic field (H) and temperature (T) plane under both ambient and applied pressure⁷. In the SC energy gap structure probed by several thermodynamic measurements⁷⁻⁹ a pair of point nodes is situated along the a -axis in orthorhombic crystal. The time reversal symmetry is broken in the SC phase detected by the Kerr rotation experiment¹⁰. The scanning tunneling microscopy (STM) experiment suggests that the chiral SC may be realized¹¹.

According to a series of ^{125}Te NMR experiments¹²⁻¹⁶, the Knight shift (KS) or the spin susceptibility drops (remains uncharged) along the b -axis and c -axis (the a -axis) below the SC transition temperature T_c at low fields, showing that the d-vector points perpendicular to the a -axis. Namely the d-vector has the components along the b and c -axes. At the lowest fields along the b -axis the KS decreases, but as H increases from 5T up to $\sim 12\text{T}$ the KS as a function of H gradually ceases decreasing to return to the normal value. This implies that the d-vector changes its direction so as to be perpendicular to the applied field direction parallel to the b -axis in order to gain the Zeeman energy. Along the c -axis the KS as a function of H starts increasing from the lowest field and continuously returns to the normal value at around 5T. Thus the d-vector should be the three components along all the three directions with complex numbers. In other words, the SC order parameters must have three dimensional vectorial structure with three components. This d-vector rotation phenomenon plays a crucial role

in understanding the field reinforced high field phase as mentioned shortly.

We focus in this paper particularly on the following experiments⁷:

- (1) The upper critical field H_{c2} is extremely high, reaching $\sim 70\text{T}$ compared with $T_c=1.6\text{K}\sim 2.0\text{K}$.
- (2) The H - T phase diagram along the magnetic hard b -axis consists of the two phases; low field (LSC) and high field phases (HSC) where in the HSC, $H_{c2}(T)$ has an unusual positive slope, *ie.* $dH_{c2}(T)/dT > 0$.
- (3) When tilting H toward the magnetic easy a -axis from the b -axis by small angles φ up to only $\varphi \sim 7^\circ$, the HSC quickly diminishes from the H - T phase diagram, leaving the LSC whose $H_{c2} \sim 10\text{T}$.
- (4) When the field direction changes from the b -axis toward the other magnetic hard c -axis by the angle θ measured from the b -axis, the HSC also diminishes up to a little larger angle $\theta \sim 12^\circ$, beyond which only the LSC remains. However, around $\theta \sim 35^\circ$ the isolated HSC detached from the LSC appears above the so-called metamagnetic transition field H_m at which the b -axis magnetization curve $M_b(H)$ exhibits a jump via a first order phase transition.

Since there is neither quantitative, nor qualitative explanation on those remarkable facts on UTe_2 , we try to understand some of these phenomena theoretically in a qualitative level. In particular, we address the following issues:

- (A) What determines the upper limit of H_{c2} ? In a clean limit superconductor¹⁷, which we assume here, the orbital limit of H_{c2} without the Pauli paramagnetic effect is given by $H_{c2}^{\text{orb}} = \Phi_0/2\pi\xi^2$ with Φ_0 the flux quantum where the coherent length $\xi = \hbar v_F/\pi T_c$. The Fermi velocity v_F measured recently by the dHvA experiment¹⁸ is $v_F^\alpha \sim 11.0\text{km/s}$ and $v_F^\beta \sim 6.3\text{km/s}$, yielding $H_{c2}^{\text{orb}} \sim 12\text{T}$. This nicely matches $H_{c2} \sim 10\text{T}$ for the LSC, but is far less than the observed maximal $H_{c2}(\theta = 35^\circ) \sim 70\text{T}$. Note that according to the H_{c2} analysis by Rosuel et al¹⁹

and Helm et al²⁰, the estimated v_F in order to explain $H_{c2} \sim 70\text{T}$ is $6.7 \sim 7.1\text{km/s}$ albeit $T_c \sim 3\text{K}$, meaning that the high and low field phases are governed by the same Fermi surface structure. Thus we need to understand a mechanism on what causes the violation of the orbital depairing limit.

(B) Why does $H_{c2} \parallel \mathbf{b}$ in the HSC have a positive slope and terminates abruptly just at $H_m = 34\text{T}$ and reappears above H_m around $\theta = 35^\circ$ intermediate between the b -axis and c -axis¹⁹⁻²¹? Why is it not between the b -axis and a -axis?

In this paper to address those issues, we assume a spin-triplet pairing with a non-unitary form²² characterized by a complex d-vector with three components. This non-unitary state quite successfully describes not only UTe_2 , but also other SC including URhGe and UCoGe . Those are all magnetization-tuned superconductors in common²³⁻²⁵.

This paper is arranged as follows. First we briefly describe our non-unitary triplet theory developed previously²³⁻²⁵ in the next section II. In order to understand a mechanism of the violation of the orbital depairing limit of H_{c2} we employ a simple Ginzburg-Landau formalism to illustrate our basic idea as clearly as possible in Section III. The proposed mechanism is applied to UTe_2 . We analyze a variety of experimental data on the H - T phase diagrams for various field orientations in Section IV. We devote to discussions and perspectives in order to deepen our understanding on the physics associated with UTe_2 and other sister compounds, URhGe and UCoGe . The topics include the classification scheme of the pairing symmetry, the concept of the d-vector rotation, possible chiral-nonchiral transition in high field in Section V. Section VI is summary and conclusion.

II. THEORETICAL FRAMEWORK

A. Preliminaries to Ginzburg-Landau theory

In order to answer the above questions (A) and (B) we start with the most generic Ginzburg-Landau (GL) theory for a spin triplet state. Here we briefly summarize our previous theory for further developments²³⁻²⁵.

We assume a non-unitary A-phase like pairing state described by the complex \mathbf{d} -vector

$$\mathbf{d}(k) = \phi(k)\boldsymbol{\eta} = \phi(k)(\boldsymbol{\eta}' + i\boldsymbol{\eta}'') \quad (1)$$

($\boldsymbol{\eta}'$ and $\boldsymbol{\eta}''$ are real vectors) among the odd-parity pairing states. $\phi(k)$ is the orbital part of the pairing function which is not specified in the main part of this paper because its form is irrelevant for the present arguments. The pairing function is classified under the overall symmetry

$$SO(3)^{\text{spin}} \times D_{2h}^{\text{orbital}} \times U(1)^{\text{gauge}} \quad (2)$$

with the spin, orbital and gauge symmetry respectively.^{26,27} We assume the weak spin-orbit coupling scheme^{28,29}. This assumption is justified by the fact that the d-vector rotation starts from the low fields, $\sim 1\text{T}$ for the c -axis¹⁴, and $\sim 5\text{T}$ for the b -axis¹³, indicating that the spin-orbit coupling is weak which locks the d-vector to crystalline lattices. This $SO(3)^{\text{spin}}$ triple spin symmetry is expressed in terms of a complex three component vectorial order parameter $\boldsymbol{\eta} = (\eta_a, \eta_b, \eta_c)$.

Under D_{2h}^{orbital} symmetry the most general Ginzburg-Landau free energy functional up to the quadratic order is expressed by

$$F^{(2)} = a_0(T - T_{c0})\boldsymbol{\eta} \cdot \boldsymbol{\eta}^* + b|\mathbf{M} \cdot \boldsymbol{\eta}|^2 + i\kappa\mathbf{M} \cdot \boldsymbol{\eta} \times \boldsymbol{\eta}^* \quad (3)$$

with b being a positive constant. The last invariant comes from the non-unitarity of the pairing function in the presence of the spontaneous moment $\mathbf{M}(H)$, which is to break the $SO(3)^{\text{spin}}$ spin symmetry. We assume $\kappa > 0$ without loss of generality, but we warn that it could be negative in UTe_2 . This term responds to external field directions differently

It is convenient to introduce

$$\eta_{\pm} = \frac{1}{\sqrt{2}}(\eta_b \pm i\eta_c) \quad (4)$$

for $\mathbf{M} = (M_a, 0, 0)$ where we define the a -axis as the magnetic easy axis. η_+ (η_-) corresponds to the spin up-up (down-down) pair, or the $A_1(A_2)$ phase. Note that the spin quantization axis is defined relative to the \mathbf{M} direction, namely, the magnetic easy a -axis here. Due to the magnetic coupling term $i\kappa\mathbf{M} \cdot \boldsymbol{\eta} \times \boldsymbol{\eta}^*$, the spin direction for the Cooper pair may change.

From Eq. (3) the quadratic term $F^{(2)}$ becomes

$$F^{(2)} = a_0\{(T - T_{c1})|\eta_+|^2 + (T - T_{c2})|\eta_-|^2 + (T - T_{c3})|\eta_a|^2\} \quad (5)$$

with

$$\begin{aligned} T_{c1,2}(M_a) &= T_{c0} \pm \frac{\kappa}{a_0}M_a, \\ T_{c3}(M_a) &= T_{c0} - \frac{b}{a_0}M_a^2. \end{aligned} \quad (6)$$

Note that the actual second transition temperature is modified to $T'_{c2} = T_{c0} - (\kappa M_a/a_0)(\beta_1 - \beta_2)/2\beta_2$ because of the fourth order GL terms²³⁻²⁵, but we ignore this correction and maintain the expression of Eq. (6) for clarity of our arguments.

The root mean square average $\sqrt{\langle M_a^2 \rangle}$ of the FM fluctuations along the magnetic easy a -axis is simply denoted by M_a and acts to shift the original transition temperature T_{c0} and split it into T_{c1} , T_{c2} , and T_{c3} expressed by Eq. (6). According to this, T_{c1} (T_{c2}) increases (decreases) linearly as a function of M_a while T_{c3} decreases

quadratically as M_a^2 from the degeneracy point $M_a = 0$. The three transition lines meet at $M_a=0$ where the three components η_i ($i = +, -, a$) are all degenerate. Thus away from the degenerate point at $M_a=0$, the A_0 phase starts at T_{c3} quickly disappears from the phase diagram. Below T_{c2} (T_{c3}) the two components η_+ and η_- coexist, symbolically denoted by A_1+A_2 . Note that because their transition temperatures are different, A_1+A_2 is not the so-called A-phase which is unitary, but generically non-unitary except at the degenerate point $M_a=0$ where the totally symmetric phase is realized with time reversal symmetry preserved. Thus the A_1+A_2 phase is the so-called distorted A phase¹. Likewise below T_{c3} all the components coexist; $A_1+A_2+A_0$ realizes.

The magnetic coupling κ , which is a key parameter to characterize UTe_2 in the following, is originally estimated³⁰ as $\kappa = T_c \frac{N'(0)}{N(0)} \ln(1.14\omega/T_c)$, with $N'(0)$ the energy derivative of the normal DOS and ω the energy cut-off. This term comes from the electron-hole asymmetry near the Fermi level. κ indicates the degree of this asymmetry. This may be substantial for a narrow band, or the Kondo coherent band in the heavy Fermion material UTe_2 . We can estimate $N'(0)/N(0) \sim 1/E_F$ with the Fermi energy E_F . Because $T_c=2mK$ and $E_F=1K$ in 3He , $\kappa \sim 10^{-3}$, while for UTe_2 $T_c \sim 1K$ and $E_F \sim T_K$ with the Kondo temperature $T_K \sim 30K$ ⁷. $\kappa \sim 10^{-1}$. We also note that the sign of κ can be either positive or negative, depending on the detailed energy dependence at the Fermi level because it is $\propto N'(0)$. If $\kappa > 0$ ($\kappa < 0$), the up-up (down-down) pair appears at higher T . Thus the Knight shift remains unchanged (decreases) below T_{c1} .

In the following discussions we consider the case where the two components η_+ and η_- are nonvanishing, ignoring the third component η_a since under ambient pressure UTe_2 exhibits the two phases LSC and HSC, corresponding to η_+ and η_- respectively. Note, however, that under pressure the third component becomes relevant²⁴. We redefine the notation $\kappa/a_0 \rightarrow \kappa$ from now on.

III. UPPER CRITICAL FIELD

Under an applied field with the vector potential \mathbf{A} , the gradient GL energy is given under D_{2h}^{orbital} symmetry

$$F_{grad} = \sum_{\nu=a,b,c} \{K_a |D_x \eta_\nu|^2 + K_b |D_y \eta_\nu|^2 + K_c |D_z \eta_\nu|^2\} \quad (7)$$

where K_a , K_b , and K_c are the effective mass along the a , b , and c -axes. $D_i = -i\nabla_i + \frac{2\pi}{\Phi_0} A_i$ is the gauge invariant derivative with Φ_0 being the quantum flux and A_i the vector potential component. We emphasize as seen from this form of Eq. (7) that H_{c2} for the three components each starting at T_{cj} ($j = 1, 2, 3$) intersects each other, never avoiding or leading to a level repulsion. The level repulsion may occur for the pairing states belonging to multi-dimensional representations (see for example [32–35] in UPt_3). The external field H comes in also through

$M_a(H)$ in addition to the vector potential \mathbf{A} which gives rise to the orbital depairing.

Thus each component is independent within the quadratic terms. The Ginzburg-Landau free energy density F under external magnetic field H in terms of the SC order parameter η_\pm given by

$$F = \sum_{i=\pm} \{a_0(T - T_{c,i})|\eta_i|^2 + K_a |D_x \eta_i|^2 + K_b |D_y \eta_i|^2 + K_c |D_z \eta_i|^2\}. \quad (8)$$

The variation with respect of η_i^* leads to the Ginzburg-Landau equation

$$a_0(T - T_c)\eta_i + (K_a D_x^2 + K_b D_y^2 + K_c D_z^2)\eta_i = 0. \quad (9)$$

Following the standard procedure³⁶, the upper critical field H_{c2} is obtained as the lowest eigenvalue of the linearized Ginzburg-Landau equation, or Schrödinger type equation of a harmonic oscillator, namely,

$$\begin{aligned} H_{c2,j}^{(+)}(T) &= \alpha_0^j(T_{c0} + \kappa M_a - T) \\ H_{c2,j}^{(-)}(T) &= \alpha_0^j(T_{c0} - \kappa M_a - T) \end{aligned} \quad (10)$$

with $j=a, b$ and c -axis. We have introduced the coefficients,

$$\begin{aligned} \alpha_0^a &= \frac{\Phi_0}{2\pi\sqrt{K_b K_c}} a_0, & \alpha_0^b &= \frac{\Phi_0}{2\pi\sqrt{K_c K_a}} a_0, \\ \alpha_0^c &= \frac{\Phi_0}{2\pi\sqrt{K_a K_b}} a_0. \end{aligned} \quad (11)$$

Those coefficients determine the initial slopes of the upper critical fields. $H_{c2,j}^{(+)}$ and $H_{c2,j}^{(-)}$ are the upper critical fields for the spin up-up and down-down pair, or the A_1 and A_2 phase respectively.

The above equation (10) is cast into a generic form:

$$H_{c2} - \alpha_0 \kappa M(H_{c2}) = \alpha_0(T_{c0} - T). \quad (12)$$

The right hand side of Eq.(12) is nothing but

$$H_{c2}^{\text{orb}}(T) = \alpha_0(T_{c0} - T) \quad (13)$$

for unperturbed upper critical field due to the orbital depairing limit with T_{c0} whose maximum value is given by $H_{c2}^{\text{orb}}(T=0) = \alpha_0 T_{c0}$. On the left hand side of Eq.(12) we define the effective field

$$H_{\text{eff}} = H_{\text{ext}} - \alpha_0 \kappa M(H_{\text{ext}}). \quad (14)$$

This implies that the external field H_{ext} is reduced by the amount of $\alpha_0 \kappa M(H_{\text{ext}})$. The upper bound of the orbital

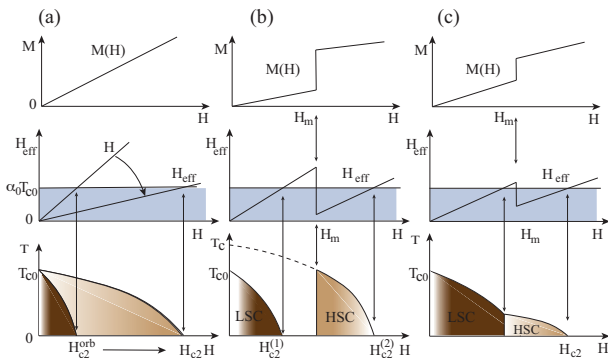


FIG. 1: (a) In the case of magnetization curve $M(H) = \chi H$ (upper panel). H_{eff} is reduced compared with the external field. The allowed region with grey color bounded by $\alpha_0 T_{c0}$ extends to a higher field (middle panel). H_{c2} is enhanced compared with H_{c2}^{orb} (the bottom panel). (b) When the magnetization has the jump at the metamagnetic field H_m , H_{eff} becomes outside of the allowed region at $H_{c2}^{(1)}$. But it comes back above H_m and HSC appears, separated from LSC. The extrapolated T_c for HSC is higher than T_{c0} for LSC (dotted curve in the bottom panel). (c) The metamagnetic jump is smaller than the case (b). LSC and HSC are overlapped to appear. The grey regions in the middle panels in (a), (b), and (c) show the allowed region for H_{c2} .

depairing field of $H_{c2}^{\text{orb}}(T)$ for the a -axis, for example, is determined by

$$H_{c2}^{\text{orb}}(T \rightarrow 0) = \alpha_0^a T_{c0} = \frac{\Phi_0}{2\pi\sqrt{K_b K_c}} a_0 T_{c0}. \quad (15)$$

This is given in turn by the expression in the clean limit: $H_{c2}^{\text{orb}}(T) = \Phi_0/2\pi\xi^2$ with the coherence length $\xi = \hbar v_F/\pi T_{c0}$. Namely, at $H_{c2}^{\text{orb}}(0)$ the inter-vortex distance becomes comparable to the core size ξ . This gives rise the absolute value of the upper limit of $H_{c2}^{\text{orb}}(0)$ in general. In order to break this absolute upper limit due to the orbital depairing, the effective magnetic field H_{eff} must be reduced from the external field H_{ext} . This idea is the same as in the case developed for a spin singlet pairing³⁷ and somewhat similar to the so-called Jaccarino-Peter mechanism³⁸. From now on we suppress subscript “ext”, thus $H_{\text{ext}} \rightarrow H$.

It is clear to see that at $T = 0$ the absolute value of H_{eff} is bounded by

$$|H_{c2} - \alpha_0 \kappa M(H_{c2})| \leq H_{c2}^{\text{orb}}(T = 0) = \alpha_0 T_{c0} \quad (16)$$

for $H_{c2}(0)$ to be a solution. Thus $H_{c2}(0)$ could be enhanced at $T \rightarrow 0$.

Let us now examine the typical cases for several magnetization curves as shown in Fig. 1. We first consider the simplest case where the magnetization curve is given by $M(H) = \chi H$ as displayed in the upper panel of Fig. 1(a). Since H_{eff} is reduced by the presence of $M(H)$ in Eq. (14) (the middle panel in Fig. 1(a)), we find

$$H_{c2}(T) = \frac{H_{c2}^{\text{orb}}(T)}{1 - \alpha_0 \kappa \chi} \quad (17)$$

$1 - \alpha_0 \kappa \chi$ is the enhancement factor relative to $H_{c2}^{\text{orb}}(T)$ (the bottom panel in Fig. 1(a)). Thus in principle $H_{c2}(T)$ increases indefinitely toward the critical point $\alpha_0 \kappa \chi = 1$ from below. As a general tendency, when the magnetization becomes saturated at higher field, $H_{c2}(T)$ eventually tends to be finite.

Next we consider the case where the magnetization curve has a jump at the metamagnetic transition at H_m as shown in the upper panel of Fig. 1(b). H_{eff} exceeds the allowed maximum region set by $\alpha_0 T_{c0}$ in Eq. (14) at a lower field as shown in the middle panel of Fig. 1(b), thus low SC (LSC) phase is terminated at $H_{c2}^{(1)}(T)$ (see the bottom panel of Fig. 1(b)). However, just above H_m , H_{eff} enters again the allowed region with grey color in the middle panel, thus high SC (HSC) appears from H_m to $H_{c2}^{(2)}(T)$ as shown in the bottom panel of Fig. 1(b). In this case LSC and HSC are separated in H - T phase diagram shown in the bottom panel in Fig. 1(b).

Depending on the magnetization curve with the metamagnetic transition, the different situation may occur as shown in Fig. 1(c). Since H_{eff} defined in Eq. (14) is determined by the combination of $M(H)$ and the coupling constant $\alpha_0 \kappa$, two SC phases of LSC and HSC are overlapped as shown in the bottom panel of Fig. 1(c). This is contrasted with the case mentioned above where LSC and HSC are separated by the normal state along the H axis in H - T phase diagram. Notice that in those examples LSC and HSC are the same pairing state.

IV. ANALYSIS OF $H_{c2}(T)$ IN UTe_2

A. $H \parallel b$

In this section, we examine the H - T phase diagram in UTe_2 for $H \parallel b$ by applying the previous general considerations based on GL theory for non-unitary pairing. In order to explain various mysteries associated with the phase diagram for $H \parallel b$, it is essential to know the magnetization curve $M(H)$ in $H \parallel b$. According to the measurement by Miyake et al³⁹ $M(H)$ has the metamagnetic transition at $H_m = 34\text{T}$ via a first order with the large magnetization jump, which is shown by the red curve of M_b in Fig. 2(b). Accordingly, the effective field H_{eff} shown by the green curve there exhibits a sharp drop at H_m . By choosing an appropriate parameter value for $\alpha_0 \kappa$ which is only the adjustable parameter in our theory, we can reproduce the experimental data. Namely, H_{eff} is reduced below $H < H_m$ as seen by the green curve of Fig. 2(b). However, beyond H_m it exceeds the limit of the allowed region denoted by the grey band.

In Fig. 2(a) the A_1 phase starts at T_{c1} and disappears at a lower field because the Cooper pair polarization

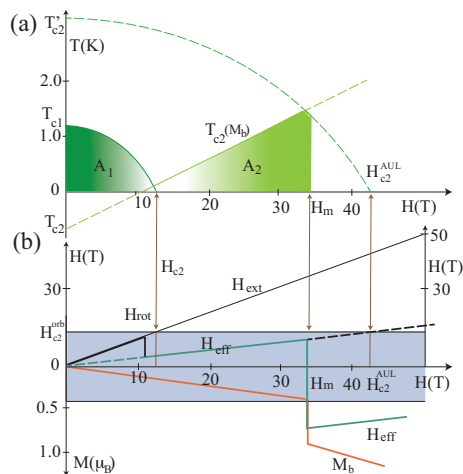


FIG. 2: (a) The resulting H - T phase diagram with the A_1 (LSC) and A_2 (HSC) phases. The dashed lines are not realized. (b) The constructed H_{eff} (green curve) at $T = 0$ as a function of the external field H using the measured magnetization curve³⁹ of $M_b(\mu_B)$ (red curve). H_{rot} is the d-vector rotation field. H_m is the metamagnetic transition field. H_{c2}^{AUL} is the absolute upper limit of H_{c2} .

points to the a -axis evidenced by the KS experiment^{12–16}. In low fields KS remains unchanged (drops) for the a -axis (b - and c -axis) field. Thus for the A_1 phase $H_{\text{eff}} = H$ because of $\mathbf{d} \times \mathbf{d}^* \perp M_b$.

On the other hand, the A_2 phase with the increasing T_{c2} changes the d-vector direction during the d-vector rotation for the field range $5\text{T} \sim 12\text{T}$ in order that $\mathbf{d} \times \mathbf{d}^* \parallel M_b$, thus now $T_{c2} = T_{c0} + \kappa M_b(H)$ instead of M_a originally given in Eq. (6), or T_{c2} increases with $M_b(H)$ as shown in Fig. 2(a). However, even if T_{c2} is increasing indefinitely, the A_2 phase ceases to exist above H_m because H_{eff} exceeds the limit. It terminates at H_{c2}^{AUL} where as shown in the dotted line of Fig. 2(b) the extrapolated H_{eff} from below exceeds the limit. This defines the absolute upper limit of H_{c2} , or H_{c2}^{AUL} , which is given by $H_{c2}^{\text{AUL}} = \alpha_0(T'_{c2} - T)$ where T'_{c2} is not realized. Note that as seen from Fig. 2(a) a part of $H_{c2}^{\text{AUL}}(T)$ is realized where H_{eff} is still within the allowed region. Those constitute the whole A_2 phase shown in Fig. 2(a).

B. b to a

When the magnetic field is tilted from the magnetic hard b -axis toward the magnetic easy a -axis by the angle φ measured from b , the HSC phase quickly diminishes from the H - T phase diagram up to $\varphi \sim 7^\circ$ while LSC remains the same. In order to understand this intriguing behaviors, we apply the same idea above by postulating the $M_b(\varphi)$ as a function of φ . When tilting the field direction away from the b -axis, $M_b(\varphi)$ generally decreases because M_b component projecting onto the field direction becomes small. Therefore, $H_{\text{eff}}(\varphi)$ increases with φ

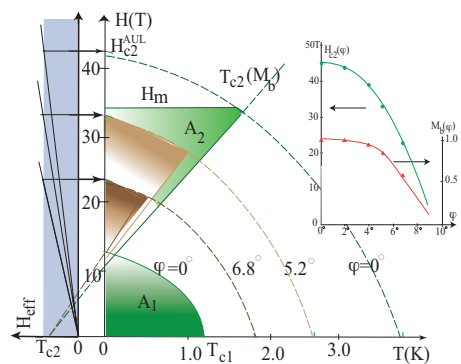


FIG. 3: The phase diagram in H - T plane for $H \parallel b$ and the field orientations tilted by the angle φ measured from the b -axis toward the a -axis. The A_2 or HSC quickly shrinks as φ increases while A_1 or LSC remains almost unaffected. $H_{c2}^{\text{AUL}}(\varphi)$ becomes low as φ increases indicated by left hand side because the projection of $M_b(\varphi)$ strongly decreases as postulated in the inset. The resulting upper critical field $H_{c2}(\varphi)$ is shown there.

as shown in the left hand side of Fig. 3, implying that $H_{c2}^{\text{AUL}}(\varphi)$ is lowered. The resulting $H_{c2}^{\text{AUL}}(\varphi)$ is plotted by the dotted curves in Fig. 3 for the selected angles. Since $T_{c2}(\varphi) = T_{c0} + \kappa M_b(\varphi)$ becomes sharper to rise or $T_{c2}(\varphi)$ at T_{c2} rotates counterclockwise as depicted in Fig. 3, the A_2 regions with the triangle areas (brown color) become shrink and disappears from the H - T phase diagram.

The postulated $M_b(\varphi)$ behavior in order to reproduce the phase diagram is depicted in the inset of Fig. 3, which is far from that expected by simple projection of $M_b(\varphi)$ onto the field direction. $M_b(\varphi)$ decreases quickly upon tilting by a few degrees, which is quite noteworthy. This might be understandable because the magnetic easy a -axis is special; The moment M_b tends to redirect toward the easy a -axis in order to gain the magnetic energy by increasing the M_a component, thus the rotation of the moment direction of M_b may be larger than the simple projection count. A similar large change of the magnetization curve by small tiltings of the field direction is observed in URhGe from the hard to easy axis case⁴⁰. Reflecting the strong decrease of $M_b(\varphi)$, the resulting $H_{c2}(\varphi)$ sharply drops as depicted in the inset of Fig. 3.

C. b to c

We examine the phase diagram for the field orientation tilted from the b -axis to the other hard axis c -axis by the angle θ measured from the b -axis to understand the isolated HSC phase whose maximum H_{c2} reaches $\sim 70\text{T}$ far above the orbital depairing upper critical field.

Let us start to evaluate the magnetization curves $M_b(\theta)$ for the arbitrary angle θ , which is a key quantity to determine H_{c2} . It is rather easy to reconstruct $M_b(\theta)$ from the magnetization curve M_b which is measured³⁹

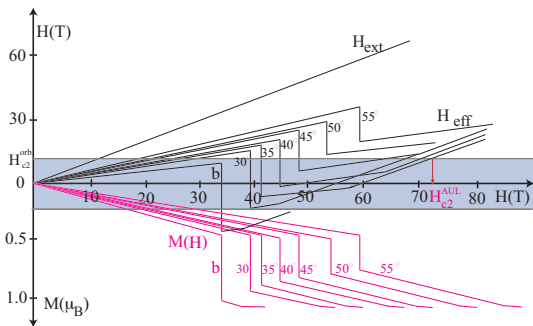


FIG. 4: The magnetization curve $M_b(H)$ (the red curve) for $H \parallel b$ -axis obtained experimentally³⁹. The other magnetization curves for various angles of θ are reconstructed by projecting $M_b(H)$ onto the magnetic field direction. $H_{\text{eff}}(\theta) = H - \alpha_0\kappa M(\theta)$ is constructed from $M(\theta)$ thus obtained. The grey color band at the center indicates the allowed region for H_{c2} . The intersection point between $H_{\text{eff}}(\theta)$ and the grey band yields the absolute upper limit H_{c2}^{AUL} .

since we know the experimental fact that $H_m \propto 1/\cos\theta$. This means that the projection of M_b onto the field direction determines the magnetization curve for $M_b(\theta)$. Therefore, by projecting M_b onto the field direction we obtain $M_b(\theta)$ for arbitrary angle. In Fig. 4, $M_b(\theta)$ is depicted as the red curves for the relevant angles of θ . We can check this procedure for the experimental data $M_b(\theta \sim 23^\circ)$ for $H \parallel (011)$ -direction³⁹ by subtracting the contribution from the magnetization component along the c -axis $M_c(\theta)$.

Using those magnetization curves and the same parameter value for $\alpha_0\kappa$, we obtain $H_{\text{eff}}(\theta) = H - \alpha_0\kappa M(\theta)$ as shown in Fig. 4. It is seen from this that for $\theta \geq 30^\circ$ the lower edge of $H_{\text{eff}}(\theta)$ begins entering the allowed region, yielding the HSC up to H_{c2}^{AUL} . Upon further increasing θ , $H_{\text{eff}}(\theta)$ is leaving this region, thus there is no HSC for $\theta > 50^\circ$.

We can construct the H - T phase diagram for θ shown in Fig. 5 where the selected θ cases are displayed, including $H \parallel b$ -axis for comparison. The left side bar denotes $H_{\text{eff}}(\theta)$ explained above. For $\theta = 12^\circ$ the A_2 phase barely remains beyond which there is no trace of the A_2 phase below H_m in the phase diagram. This is because $T_{c2}(M_b)$ curves (denoted in the dotted straight lines in Fig. 5) starting at T_{c2} for $H = 0$ rotate counter-clockwise due to the decrease of the M_b projection. However for $\theta = 35^\circ$ this T_{c2} line still reaches the metamagnetic transition field, which allows the HSC to exist above H_m as shown in Fig. 5. Thus starting from $H_{c2}^{\text{AUL}} \sim 70\text{T}$ through H_m , the H_{c2} curve is extended toward $T_{c2} \sim 3\text{K}$ at $H=0$. However the actual HSC phase disappears abruptly at H_m because H_{eff} is outside of the allowed region below H_m . For $\theta = 45^\circ$ since there is only tiny field region allowed for H_{eff} as seen from the left hand side of Fig. 5, the resulting HSC region in the H - T phase diagram shrinks. There is no HSC allowed for $\theta = 50^\circ$. Those features are displayed in the inset of Fig. 5.

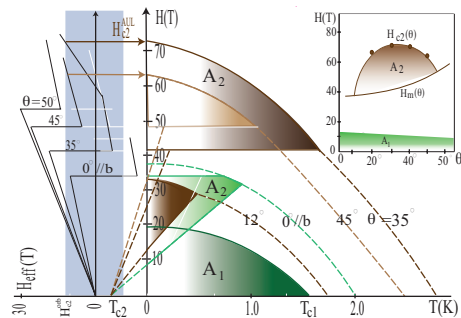


FIG. 5: The H - T phase diagram for various θ , including the case $H \parallel b$ -axis for comparison. The allowed region of H_{eff} is displayed in the left hand side by grey color, which is the same as in Fig. 4. For $\theta = 35^\circ$ the HSC (A_2) is allowed for $H_m < H_{\text{eff}} < H_{c2}^{\text{AUL}}$. The H_{c2} curve starts at H_{c2}^{AUL} toward T_{c2} at $H = 0$. But the HSC terminates abruptly at H_m below which H_{eff} is outside of the allowed region. The allowed region at the low field is not available for the A_2 because $T_{c2} < 0$ there. It is used by the LSC (A_1), which is relatively unchanged in varying θ , including the case $H \parallel b$ -axis. The inset shows the HSC (A_2) and LSC (A_1) as a function of θ .

V. DISCUSSIONS AND PERSPECTIVES

A. Parameter value of $\alpha_0\kappa$

We examine the parameter values used in this paper. The key parameter in this work is the product $\alpha_0\kappa$ of α_0 introduced in Eq. (11) and κ defined in Eq. (3). We ignore the small anisotropy of the initial slopes of H_{c2} at T_c for three field orientations of the a -, b -, and c -axes. From the initial slopes, we find $\alpha_0 = 12\text{T}/1.6\text{K} = 7.5\text{T/K}$. From the previous estimate $\kappa = 6.9\text{K}/\mu_B$ ²⁵, which is determined by the splitting between T_{c1} and T_{c2} and the amplitude of the ferromagnetic fluctuation moment along the a -direction. We obtain $\alpha_0\kappa = 51.8\text{T}/\mu_B$. From Eq. (14) it is seen that

$$H_{\text{eff}} = H - \alpha_0\kappa M = H - J_{\text{cf}}M, \quad (18)$$

namely, this combination is nothing but the form of the exchange integral J_{cf} between the $5f$ localized moment and conduction electrons, *ie.* $J_{\text{cf}} = \alpha_0\kappa$.

It is interesting to notice the case in the recently found heavy Fermion superconductor CeRh_2As_2 ⁴¹ where $H_{c2} = 16\text{T}$ and $T_c = 0.35\text{K}$. This compound is known to break the Pauli-Clogston limit $H_p = 1.84T_c \sim 0.6\text{T}$ by far. In order to overcome this Pauli-Clogston limit for this spin singlet superconductor, we introduce the effective field $H_{\text{eff}} = H - J_{\text{cf}}M$ where the internal field is exerted from the localized $4f$ moment M to cancel the external applied field³⁷. The exchange integral is estimated as $J_{\text{cf}}^c = 52.5\text{T}/\mu_B$ ($J_{\text{cf}}^{ab} = 23.4/\mu_B$) for the c -axis (ab -plane) in tetragonal crystal. Those numbers remarkably coincide with the present system, but it may be only coincident. The important thing is that to achieve the high

H_{c2} it is necessary to break the Pauli-Clogston limit for a spin singlet superconductor or the orbital depairing limit for a spin triplet superconductor. Here we propose a common mechanism where the external field is effectively cancelled by the internal field due to the moments of the localized f electrons through the exchange coupling to the itinerant electron system.

B. Pairing symmetry of UTe₂ and classification scheme

The present analysis clearly shows that the non-unitary state in the chiral form $d(k) = (b + ic)(k_b + ik_c)$ is best suitable for UTe₂. Here we chose the orbital part $\phi(k) = k_b + ik_c$. Under applied fields the d-vector rotates so as to save the Zeeman energy. This means that the spin-orbit coupling to lock the d-vector to the underlying crystal lattices is weak and finite. Namely, the d-vector rotation fields H_{rot} depend on the field orientation, that is, $H_{\text{rot}} = 5 \sim 12\text{T}$ for $H \parallel b$ -axis and $H_{\text{rot}} = 1\text{T}$ for $H \parallel c$ -axis. Those weak fields of H_{rot} indicate the strength of the spin-orbit coupling (SOC). Therefore we have to resort to the weak SOC scheme for the pairing symmetry classification.

The spin-orbit coupling is anisotropic, thus the spin space symmetry for the Cooper pairs is weakly broken from the original $\text{SO}(3)^{\text{spin}}$. Furthermore, the slow ferromagnetic fluctuations also break it to split the SC transition temperature into three, T_{c1} , T_{c2} , and T_{c3} . In this way we can reasonably identify the relevant Cooper pair symmetry started from $\text{SO}(3)^{\text{spin}}$, which is decoupled with the orbital part of the pairing function in this scheme. We emphasize that since in the strong SOC case advocated by others⁴²⁻⁴⁵ the spin space symmetry and the orbital space symmetry are tightly coupled, there is no freedom to allow the d-vector rotation. As mentioned above the gradual rotation of the d-vector via a second order phase transition is accounted for only by the weak SC case. As for the orbital symmetry governed by the crystalline symmetry D_{2h} , there is no multi-dimensional representation. Thus the choice of the chiral form $k_b + ik_c$ which is consistent with many experiments⁷⁻⁹ is ad hoc at this stage. It may be that the classification scheme based on the D_{2h} crystalline symmetry turns out to be irrelevant and more larger symmetry group is needed. Note that a convex curve behavior of the Sommerfeld coefficient $\gamma(H)$ at low fields for $H \parallel b$ -axis associated with the Pauli paramagnetic effect⁴⁶ is an important signature of the d-vector locking and should be checked experimentally.

C. d-vector rotation

The d-vector rotation is an important concept for describing the phenomena associated with peculiar H - T phase diagrams. In particular for $H \parallel b$ -axis the positive

slope above $H \simeq 12\text{T}$ can be accounted for by the d-vector rotation where the d-vector becomes perpendicular to the b -axis so that the magnetic coupling $i\mathbf{M}_b \cdot \mathbf{d} \times \mathbf{d}^*$ is active and fully takes advantage from this magnetic energy, otherwise this invariant does not help to raise T_{c2} . In this sense the d-vector rotation is essential to capture this phenomenon.

Microscopically the d-vector rotation occurs as a change of the spin texture formed by the spatial modulation of the three dimensional d-vector, or the Cooper pair spin polarization defined by $\mathbf{S}(r) = i\mathbf{d} \times \mathbf{d}^*$. The averaged $\mathbf{S}(r)$ over the vortex unit cell determines the direction of the d-vector. The d-vector rotation is induced because the competition between the Zeeman energy and the pinning of the d-vector to the underlying lattices due to the SOC. A microscopic theory based on quasi-classical Eilenberger equation is now in progress where intriguing spin textures, including a pair of the half-quantized vortices and Majorana zero modes both with spinless and spinfull are stabilized⁴⁷.

D. Chiral-nonchiral transition and β phase

When the magnetic field $H \parallel b$ -axis is applied to the fully polarized nonunitary chiral p state $(a + ic)(k_b + ik_c)$, the chiral-nonchiral transition may occur. This mechanism is originally proposed by Scharnberg-Klemm⁴⁸. This is simply because to compare the two upper critical fields for the chiral state $(a + ic)(k_b + ik_c)$ and the nonchiral state $(a + ic)k_b$ the latter has higher H_{c2} in general, a factor ~ 1.5 higher for the spherical Fermi surface⁴⁹. The line node in $(a + ic)k_b$ is robust under fields compared with $(a + ic)(k_b + ik_c)$ having the point nodes. This nonchiral state $(a + ic)k_b$ is named as the so-called β phase^{1,28,29}. The β phase produced by high magnetic fields from the polar phase is recently identified in superfluid ³He confined in nematic aerogel⁵⁰. Thus it is quite interesting to investigate this possibility further in our superconductor. We have already identified the A_1 , A_2 , $A_1 + A_2$ (distorted A), and $A_1 + A_2 + A_0$ phases in lower and intermediate field regions under ambient pressure and under pressure respectively²³⁻²⁵.

E. Application to URhGe and UCoGe

In order to examine the validity of the present theory, we apply it to other materials, ferromagnetic superconductors URhGe and UCoGe which are best systems to check our idea. Under hydrodynamic and uniaxial pressure the H - T phase diagrams in URhGe continuously change as shown in Fig. 6. The features are strikingly similar to those we have just seen, such as

- (1) $T_c(H)$ increases as H increases in some part of H - T phase diagram,
- (2) the extrapolated T_c from the high field H_{c2} to high T exceeds T_{c0} at $H = 0$,

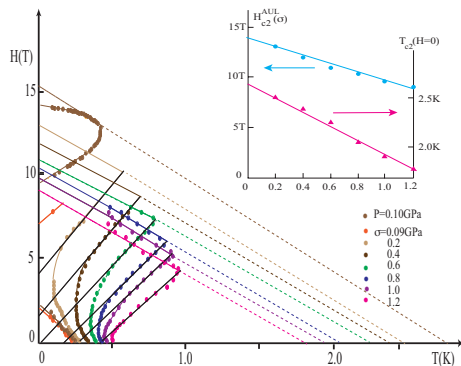


FIG. 6: H - T phase diagram under hydrodynamic (P) and uniaxial (σ) pressure for URhGe. The extrapolated straight line to lower T defines H_{c2}^{AUL} and $T_{c2}(H=0)$ to higher T respectively. The pressure dependences of H_{c2}^{AUL} and $T_{c2}(H=0)$ are shown in the inset, indicating the linear scaling for both quantities with the linear decrease of M_c . The dotted points are the experimental data^{51,52}.

- (3) the HSC is separated from LSC at low pressure,
- (4) HSC and LSC is overlapped in high pressure region.

Let us examine those features observed in URhGe in light of the present idea. It is known that under uniaxial pressure σ the spontaneous moment M_c decreases linearly and vanishes at $\sigma=1.2\text{GPa}$, namely $M_c(\mu_B) = 0.4 - 0.33\sigma(\text{GPa})$. It is reasonable to consider that $M_b(H) = \chi_b H$ where χ_b decreases in proportion with σ , namely $\chi_b = \chi_{b0} - A\sigma$ with A positive constant because the spontaneous moment M_c sets the overall magnetic scale. Thus it is expected that H_{c2}^{AUL} is given by $H_{c2} - \alpha_0 \kappa M_c = \alpha_0 T_{c0}$, or

$$\begin{aligned} H_{c2} - \alpha_0 \kappa \chi_b H_{c2} &= \alpha_0 T_{c0}, \\ H_{c2} - \alpha_0 \kappa (\chi_{b0} - A\sigma) H_{c2} &= \alpha_0 T_{c0}. \end{aligned} \quad (19)$$

The above Eq. (19) is rewritten as

$$\frac{H_{c2}(\sigma)}{H_{c2}(\sigma=0)} = \frac{1}{1 + \frac{\kappa \alpha_0 A \sigma}{1 - \kappa \alpha_0 \chi_0}} \simeq 1 - \frac{\kappa H_{c2}(\sigma=0) A \sigma}{T_{c0}}. \quad (20)$$

Namely, $H_{c2}^{\text{AUL}}(\sigma)$ decreases linearly with σ . This also implies that $T_{c2}(H=0)$ decreases linearly with σ . As displayed in the inset of Fig. 6 this relation is well obeyed.

Here we quote our previous figure²⁵ on UCoGe modified slightly as Fig. 7. It is clear that there certainly exists H_{c2}^{AUL} in UCoGe too. The extrapolated $T_{c2}(H \rightarrow 0) \sim 1.0\text{K}$ far higher than T_{c1} . The S-shaped H_{c2} is limited from the above, evidencing the presence of H_{c2}^{AUL} . We now understand the reason why it is so.

F. Perspectives

The present material UT₂ is considered to be nearly ferromagnetic although the “static” long range ferromag-

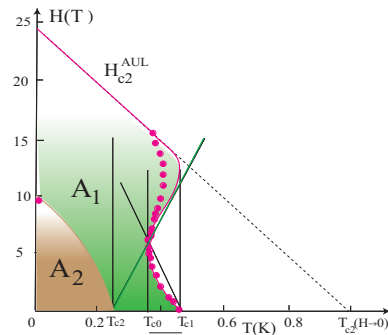


FIG. 7: H - T phase diagram²⁵ for $H \parallel b$ -axis in UCoGe. The extrapolated straight line to lower T and higher T defines $H_{c2}^{\text{AUL}} = 24T$ and $T_{c2}(H=0) = 1.0\text{K}$ respectively. The red dots are the experimental data^{53,54}.

netic (FM) ordering is absent⁵⁵. The slow FM fluctuations are reported by several experiments^{55–58}. This situation is similar to UPt₃ where the antiferromagnetic (AF) order above T_c is not truly static and long-ranged order, yet it leads to the spitting of T_c and significant effects on SC^{23–25}.

The interplay between magnetism both with FM and AF and superconductivity is an important subject and has been discussed for long time⁵⁹. Initially the case where magnetism arises from localized moments is considered. Thus the conduction electrons responsible for SC is distinctively different from the magnetic subsystem. This includes chevreil compounds (RE)Rh₄B₄ and (RE)Mo₆S₈ (RE: rare earth atoms). Magnetism affects on profound influences of SC or H_{c2} due to the onset of AF at T_N below which H_{c2} exhibits an anomalous kink structure associated with the destruction of a part of the Fermi surface by AF gapping⁶⁰. In the FM case the internal FM molecular field induces Fulde-Ferrell-Larkin-Ovchinnikov state⁶¹ just below the Currie temperature T_{Currie} .

Those examples of the coexistence clearly differ from the present generation of the intertwining problem^{62–64} in that the electrons responsible for magnetism and SC are not separable and exhibit simultaneous roles for both orderings. This duality of localized and itinerant electrons in the heavy Fermion materials is essential in forming the heavy Fermion state with the enhanced electron mass. In this case the interplay of magnetism and SC is more intricate, which is the present situation in UTe₂, but as we have seen in this paper the idea of the FM molecular field exerted from the magnetic sub-system is quite a useful concept in understanding various mysteries associated with the phase diagram constructions. This continues to be valid and profitable to apply for other heavy Fermion SC⁶⁵, including the globally or locally noncentrosymmetry broken SC such as CePt₃Si, or CeRh₂As₂. Those are known as the materials that AF coexists with SC, and the anomalously enhanced H_{c2} which breaks the Pauli-Clogston limit³⁷.

We admit that there are several outstanding issues to be solved in UTe_2 in spite of the present and previous works²³⁻²⁵.

(1) Since according to our theory the tetra-critical point exists at $H(\parallel b) \sim 13\text{T}$ as shown in Fig. 2(a), the “fourth” second order internal phase transition is still missing.

(2) The detailed phase diagram of HSC in $0 < \theta < 12^\circ$ is to be investigated because it is continuously connected to the isolated HSC around $30^\circ < \theta < 45^\circ$.

(3) The possible chiral-nonchiral transition for HSC should be checked experimentally. The β phase may be found.

(4) Magnetic elastic neutron scattering experiment can probe the magnetization $M_b(H)$ component for $0^\circ < \varphi < 8^\circ$ and $0^\circ < \theta < 45^\circ$ to establish our reconstructed magnetization curves as shown in Figs. 3 and 4. And also small angle neutron scattering (SANS) experiment is important to see vortices with the spin textures for the intermediate fields of $H \parallel b$ -axis.

(5) The vortex core contains the Majorana zero energy modes spinless or spinful for HSC and LSC respectively. Those zero Majorana modes are detected through the local density of states⁶⁶ probed by STM, or other methods.

VI. CONCLUSION AND SUMMARY

Based on a nonunitary triplet pairing state, we have found that the orbital depairing limit of H_{c2} can be ex-

ceeded by cancelling the external field via the internal field exerted from the localized moments. This novel mechanism for a spin triplet state allows us to analyze the H_{c2} phase diagrams for various field orientations centered along the magnetic hard b -axis. In particular, the record high $H_{c2} \sim 70\text{T}$ occurring in between the b -axis and the c -axis can be understood by this orbital limit violation mechanism. The present work not only has identified the pairing state realized in UTe_2 , but also proposed a novel mechanism for the violation of the orbital limit of H_{c2} , which enables us to attain higher H_{c2} in a superconductor in general.

Acknowledgments

The author is grateful for the enlightening discussions with D. Aoki, K. Ishida, S. Kitagawa, Y. Shimizu, S. Kittaka, T. Sakakibara, Y. Tokunaga, Y. Haga, H. Sakai, and A. Miyake. This work is supported by JSPS KAKENHI, No.17K05553 and No. 21K03455

-
- ¹ D. Vollhart and P. Wölfle, *The superfluid phases of Helium 3*, Taylor and Francis, London, 1990.
- ² Takeshi Mizushima, Yasumasa Tsutsumi, Takuto Kawakami, Masatoshi Sato, Masanori Ichioka, and Kazushige Machida, *Symmetry-Protected Topological Superfluids and Superconductors —From the Basics to ³He—*, *J. Phys. Soc. Jpn.* **85**, 022001 (2016).
- ³ K. Machida and M. Ozaki, *Superconducting double transition in a heavy-fermion material UPt_3* , *Phys. Rev. Lett.* **66**, 3293 (1991).
- ⁴ T. Ohmi and K. Machida, *Nonunitary superconducting state in UPt_3* , *Phys. Rev. Lett.* **71**, 625 (1993).
- ⁵ Y. Machida, A. Itoh, Y. So, K. Izawa, Y. Haga, E. Yamamoto, N. Kimura, Y. Onuki, Y. Tsutsumi, and K. Machida, *Twofold Spontaneous Symmetry Breaking in the Heavy-Fermion Superconductor UPt_3* , *Phys. Rev. Lett.* **108**, 175002 (2012).
- ⁶ Y. Tsutsumi, M. Ishikawa, T. Kawakami, T. Mizushima, M. Sato, M. Ichioka, and K. Machida, *UPt_3 as a Topological Crystalline Superconductor*, *J. Phys. Soc. Jpn.* **82**, 113707 (2013).
- ⁷ D. Aoki, J. -P. Brison, J. Flouquet, K. Ishida, G. Knebel, Y. Tokunaga, and Y. Yanase, *Unconventional Superconductivity in UTe_2* , *J. Phys.: Condens. Matter* **34**, 243002 (2022).
- ⁸ T. Metz, S. Bao, S. Ran, I-L. Liu, Y. S. Eo, and W. T. Fuhrman, D. F. Agterberg, S. Anlage, N. P. Butch, and J. Paglione, *Point node gap structure of spin-triplet superconductor UTe_2* , *Phys. Rev. B* **100**, 220504 (R) (2019).
- ⁹ Shunichiro Kittaka, Yusei Shimizu, Toshiro Sakakibara, Ai Nakamura, Dexin Li, Yoshiya Homma, Fuminori Honda, Dai Aoki, and Kazushige Machida, *Orientation of point nodes and nonunitary triplet pairing tuned by the easy-axis magnetization in UTe_2* , *Phys. Rev. Research* **2**, 032014(R) (2020).
- ¹⁰ Di S. Wei, David Saykin, Oliver Y. Miller, Sheng Ran, Shanta R. Saha, Daniel F. Agterberg, Jörg Schmalian, Nicholas P. Butch, Johnpierre Paglione, and Aharon Kapitulnik, *Interplay between magnetism and superconductivity in UTe_2* , *Phys. Rev. B* **105**, 024521 (2022).
- ¹¹ Lin Jiao, Zhenyu Wang, Sheng Ran, Jorge Olivares Rodriguez, Manfred Sigrist, Ziqiang Wang, Nicholas Butch, and Vidya Madhavan, *Microscopic evidence for a chiral superconducting order parameter in the heavy fermion superconductor UTe_2* , *Nature*, **579**, 523 (2020).
- ¹² G. Nakamine, Shunsaku Kitagawa, Kenji Ishida, Yo Tokunaga, Hironori Sakai, Shinsaku Kambe, Ai Nakamura, Yusei Shimizu, Yoshiya Homma, Dexin Li, Fuminori Honda, and Dai Aoki, *Superconducting properties of heavy fermion UTe_2 revealed by ¹²⁵Te-nuclear magnetic resonance*, *J. Phys. Soc. Jpn.* **88**, 113703 (2019).
- ¹³ Genki Nakamine, Katsuki Kinjo, Shunsaku Kitagawa, Kenji Ishida, Yo Tokunaga, Hironori Sakai, Shinsaku Kambe, Ai Nakamura, Yusei Shimizu, Yoshiya Homma, Dexin Li, Fuminori Honda, and Dai Aoki, *Inhomogeneous Superconducting State Probed by ¹²⁵Te NMR on UTe_2* , *J.*

- Phys. Soc. Japan **90**, 064709 (2021).
- 14 Genki Nakamine, Katsuki Kinjo, Shunsaku Kitagawa, Kenji Ishida, Yo Tokunaga, Hironori Sakai, Shinsaku Kambe, Ai Nakamura, Yusei Shimizu, Yoshiya Homma, Dexin Li, Fuminori Honda, and Dai Aoki, Anisotropic response of spin susceptibility in the superconducting state of UTe_2 probed with ^{125}Te -NMR measurement, Phys. Rev. B **103**, L100503 (2021).
 - 15 Hiroki Fujibayashi, Genki Nakamine, Katsuki Kinjo, Shunsaku Kitagawa, Kenji Ishida, Yo Tokunaga, Hironori Sakai, Shinsaku Kambe, Ai Nakamura, Yusei Shimizu, Yoshiya Homma, Dexin Li, Fuminori Honda, and Dai Aoki, Superconducting Order Parameter in UTe_2 Determined by Knight Shift Measurement, J. Phys. Soc. Jpn. **91**, 043705 (2022).
 - 16 K. Kinjo, H. Fujibayashi, S. Kitagawa, K. Ishida, Y. Tokunaga, H. Sakai, S. Kambe, A. Nakamura, Y. Shimizu, Y. Homma, D. X. Li, F. Honda, D. Aoki, K. Hiraki, M. Kimata, and T. Sasaki, Magnetic field-induced transition with spin rotation in the superconducting phase of UTe_2 , arXiv:2206.02444.
 - 17 It should be noted that in a dirty superconductor, H_{c2} can be arbitrarily large in principle because the effective coherent length is given by a symbolic formula $1/\xi_{\text{eff}} \propto 1/l + 1/\xi$ with l being the transport mean free path.
 - 18 D. Aoki, H. Sakai, P. Opletal, Y. Tokiwa, J. Ishizuka, Y. Yanase, H. Harima, A. Nakamura, D. Li, Y. Homma, Y. Shimizu, G. Knebel, J. Flouquet, and Y. Haga, First Observation of the de Haas-van Alphen Effect and Fermi Surfaces in the Unconventional Superconductor UTe_2 , J. Phys. Soc. Jpn. **91**, 083704 (2022).
 - 19 A. Rosuel, C. Marcenat, G. Knebel, T. Klein, A. Pourret, N. Marquardt, Q. Niu, S. Rousseau, A. Demuer, G. Seyfarth, G. Lapertot, D. Aoki, D. Braithwaite, J. Flouquet, and J. -P. Brison, Field-induced tuning of the pairing state in a superconductor, arXiv:2205.04524.
 - 20 T. Helm, M. Kimata, K. Sudo, A. Miyata, J. Stirnat, T. Förster, J. Hornung, M. König, I. Sheikin, A. Pourret, G. Lapertot, D. Aoki, J. -P. Brison, G. Knebel, and J. Wosnitza, Suppressed magnetic scattering sets conditions for the emergence of 40T high-field superconductivity in UTe_2 , arXiv:2207.08261.
 - 21 G. Knebel, W. Knafo, A. Pourret, Q. Niu, M. Vališka, D. Braithwaite, G. Lapertot, M. Nardone, A. Zitouni, S. Mishra, I. Sheikin, G. Seyfarth, J.-P. Brison, D. Aoki, and J. Flouquet, Field-reentrant superconductivity close to a metamagnetic transition in the heavy-fermion superconductor UTe_2 , J. Phys. Soc. Jpn. **88**, 063707 (2019).
 - 22 Aline Ramires, Nonunitary Superconductivity in Complex Quantum Materials, arXiv:2202.12178.
 - 23 K. Machida, Theory of Spin-polarized Superconductors—An Analogue of Superfluid ^3He A-phase—, J. Phys. Soc. Jpn. **89**, 033702 (2020).
 - 24 K. Machida, Notes on Multiple Superconducting Phases in UTe_2 –Third Transition–, J. Phys. Soc. Jpn. **89**, 0655001 (2020).
 - 25 K. Machida, Nonunitary triplet superconductivity tuned by field-controlled magnetization: URhGe , UCoGe , and UTe_2 , Phys. Rev. B **104**, 014514 (2021).
 - 26 K. Machida and T. Ohmi, Phenomenological theory of ferromagnetic superconductivity, Phys. Rev. Lett. **86**, 850 (2001).
 - 27 J. F. Annett, Symmetry of the order parameter for high-temperature superconductivity, Adv. Phys. **39**, 83 (1990).
 - 28 Masa-aki Ozaki, Kazushige Machida, and Tetsuo Ohmi, On p-Wave Pairing Superconductivity under Cubic Symmetry, Prog. Theor. Phys. **74**, 221 (1985).
 - 29 Masa-aki Ozaki, Kazushige Machida, and Tetsuo Ohmi, On p-Wave Pairing Superconductivity under Hexagonal and Tetragonal Symmetries, Prog. Theor. Phys. **75**, 442 (1986).
 - 30 V. Ambegaokar and N. D. Mermin, Thermal anomalies of He^3 : pairing in a magnetic field, Phys. Rev. Lett. **30**, 81 (1973).
 - 31 D. Aoki, K. Ishida, and J. Flouquet, Review of U-based Ferromagnetic Superconductors: Comparison between UGe_2 , URhGe , and UCoGe , J. Phys. Soc. Jpn. **88**, 022001 (2019).
 - 32 K. Machida, T. Ohmi, and M. Ozaki, Anisotropy of Upper Critical Fields for d- and p-Wave Pairing Superconductivity, J. Phys. Soc. Jpn. **54**, 1552 (1985).
 - 33 K. Machida, M. Ozaki, and T. Ohmi, Unconventional Superconducting Class in a Heavy Fermion System UPt_3 , J. Phys. Soc. Jpn. **59**, 1397 (1990).
 - 34 K. Machida, T. Fujita, and T. Ohmi, Vortex Structures in an Anisotropic Pairing Superconducting State with Odd-Parity, J. Phys. Soc. Jpn. **62**, 680 (1993).
 - 35 K. Machida, T. Nishira, and T. Ohmi, Orbital Symmetry of a Triplet Pairing in a Heavy Fermion Superconductor UPt_3 , J. Phys. Soc. Jpn. **68**, 3364 (1999).
 - 36 M. Tinkham, *Introduction to Superconductivity*, McGraw-Hill, New York, 1975.
 - 37 K. Machida, Violation of Pauli-Clogston limit in the heavy-fermion superconductor CeRh_2As_2 : Duality of itinerant and localized 4f electrons, Phys. Rev. B **106**, 184509 (2022).
 - 38 V. Jaccarino and M. Peter, Ultra-High-Field Superconductivity, Phys. Rev. Lett. **9**, 290 (1962).
 - 39 A. Miyake, Y. Shimizu, Y. J. Sato, D. Li, A. Nakamura, Y. Homma, F. Honda, J. Flouquet, M. Tokunaga, and D. Aoki, Metamagnetic transition in heavy Fermion superconductor UTe_2 , J. Phys. Soc. Jpn. **88**, 063706 (2019).
 - 40 Shota Nakamura, Toshiro Sakakibara, Yusei Shimizu, Shunichiro Kittaka, Yohei Kono, Yoshinori Haga, Jiří Pospíšil, and Etsuji Yamamoto, Wing structure in the phase diagram of the Ising ferromagnet URhGe close to its tricritical point investigated by angle-resolved magnetization measurements, Phys. Rev. B **96**, 094411 (2017).
 - 41 S. Khim, J. F. Landaeta, J. Banda, N. Bannor, M. Brando, P. M. R. Brydon, D. Hafner, R. KÜchler, R. Cardoso-Gil, U. Stockert, A. P. Mackenzie, D. F. Agterberg, C. Geibel, and E. Hassinger, Field-induced transition within the superconducting state of CeRh_2As_2 , Science **373**, 1012 (2021).
 - 42 P. W. Anderson, Structure of “triplet” superconducting energy gaps, Phys. Rev. B **30**, 4000 (1984).
 - 43 E. I. Blount, Symmetry properties of triplet superconductors, Phys. Rev. B **32**, 2935 (1985).
 - 44 G. E. Volovik, and L. P. Gor’kov, Superconducting classes in heavy-fermion systems Sov. Phys. JETP **61**, 843 (1985).
 - 45 R. Joynt and L. Taillefer, The superconducting phases of UPt_3 , Rev. Mod. Phys. **74**, 235.
 - 46 K. Machida and M. Ichioka, Magnetic field dependence of low-temperature specific heat in Sr_2RuO_4 , Phys. Rev. B **77**, 184515 (2008).
 - 47 Y. Tsutsumi and K. Machida, in preparation.
 - 48 K. Scharnberg and R. A. Klemm, Upper Critical Field in p-Wave Superconductors with Broken Symmetry, Phys. Rev.

- Lett. **54**, 2445 (1985).
- ⁴⁹ P. Miranović, N. Nakai, M. Ichioka, and K. Machida, Orientational field dependence of low-lying excitations in the mixed state of unconventional superconductors, *Phys. Rev. B* **68**, 052501 (2003).
- ⁵⁰ V. V. Dmitriev, M. S. Kutuzov, A. A. Soldatov, and A. N. Yudin, Superfluid β phase in liquid ^3He , *Phys. Rev. Lett.* **127**, 265301 (2021).
- ⁵¹ A. Miyake, D. Aoki, and J. Flouquet, Pressure evolution of the ferromagnetic and field re-entrant superconductivity in URhGe, *J. Phys. Soc. Jpn.* **78**, 063703 (2009).
- ⁵² D. Braithwaite, D. Aoki, J.-P. Brison, J. Flouquet, G. Knebel, A. Nakamura, and A. Pourret, Dimensionality Driven Enhancement of Ferromagnetic Superconductivity in URhGe, *Phys. Rev. Lett.* **120**, 037001 (2018).
- ⁵³ D. Aoki, T. D. Matsuda, V. Taufour, E. Hassinger, G. Knebel, and J. Flouquet, Extremely large and anisotropic upper critical field and the ferromagnetic instability in UCoGe, *J. Phys. Soc. Jpn.* **78**, 113709 (2009).
- ⁵⁴ B. Wu, G. Bastien, M. Taupin, C. Paulsen, L. Howard, D. Aoki, and J.-P. Brison, Pairing mechanism in the ferromagnetic superconductor UCoGe, *Nat. Commun.* **8**, 14480 (2017).
- ⁵⁵ S. Sundar, S. Gheidi, K. Akintola, A. M. Côté, S. R. Dunsiger, S. Ran, N. P. Butch, S. R. Saha, J. Paglione, and J. E. Sonier, Coexistence of ferromagnetic fluctuations and superconductivity in the actinide superconductor UTe₂, *Phys. Rev. B* **100**, 140502 (R) (2019).
- ⁵⁶ Yo Tokunaga, Hironori Sakai, Shinsaku Kambe, Taisuke Hattori, Nonoka Higa, Genki Nakamine, Shunsaku Kitagawa, Kenji Ishida, Ai Nakamura, Yusei Shimizu, Yoshiya Homma, DeXin Li, Fuminori Honda, and Dai Aoki, ^{125}Te -NMR study on a single crystal of heavy fermion superconductor UTe₂, *J. Phys. Soc. Jpn.* **88**, 073701 (2019).
- ⁵⁷ Yo Tokunaga, Hironori Sakai, Shinsaku Kambe, Yoshinori Haga, Yoshifumi Tokiwa, Petr Opletal, Hiroki Fujibayashi, Katsuki Kinjo, Shunsaku Kitagawa, Kenji Ishida, Ai Nakamura, Yusei Shimizu, Yoshiya Homma, Dexin Li, Fuminori Honda, and Dai Aoki, Slow Electronic Dynamics in the Paramagnetic State of UTe₂, *J. Phys. Soc. Jpn.* **91**, 023707 (2022).
- ⁵⁸ Devi V. Ambika, Qing-Ping Ding, Khusboo Rana, Corey E. Frank, Elizabeth L. Green, Sheng Ran, Nicholas P. Butch, and Yuji Furukawa, Possible Coexistence of Antiferromagnetic and Ferromagnetic Spin Fluctuations in the Spin-triplet Superconductor UTe₂ Revealed by ^{125}Te NMR under Pressure, *Phys. Rev. B* **105**, L220403 (2022).
- ⁵⁹ K. Machida, Spin Density Wave and Superconductivity in Highly Anisotropic Materials, *J. Phys. Soc. Jpn.* **50**, 2195 (1981). K. Machida and T. Matsubara, Spin Density Wave and Superconductivity in Highly Anisotropic Materials. II. Detailed Study of Phase Transitions, *J. Phys. Soc. Jpn.* **50**, 3231 (1981).
- ⁶⁰ K. Machida, K. Nokura, and T. Matsubara, Theory of antiferromagnetic superconductors, *Phys. Rev. B* **22**, 2307 (1980).
- ⁶¹ K. Machida and H. Nakanishi, Superconductivity under a ferromagnetic molecular field, *Phys. Rev. B* **30**, 122 (1984).
- ⁶² K. Machida and M. Kato, Inherent Spin-Density-Wave Instability in Heavy-Fermion Superconductivity, *Phys. Rev. Lett.* **58**, 1986 (1987).
- ⁶³ Eduardo Fradkin, Steven A. Kivelson, and John M. Tranquada, Theory of intertwined orders in high temperature superconductors, *Rev. Mod. Phys.* **87**, 457 (2015).
- ⁶⁴ B. Keimer, S. A. Kivelson, M. R. Norman, S. Uchida, and J. Zaanen, From quantum matter to high-temperature superconductivity in copper oxides, *Nature* **518**, 179 (2015).
- ⁶⁵ C. Pfleiderer, Superconducting phase of f-electron compounds, *Rev. Mod. Phys.* **81**, 1551 (2009).
- ⁶⁶ M. Ichioka, N. Hayashi, and K. Machida, Local density of states in the vortex lattice in a type-II superconductor, *Phys. Rev. B* **55**, 6565 (1997).